Am J Transl Res 2025;17(8):5871-5884
www.ajtr.org /ISSN:1943-8141/AJTR0164288

Original Article

Artemether ameliorates type 1 diabetes mellitus by modulating glycolipid metabolism in skeletal muscle

Yifan Dong[1*], Qike Fu[2*], Yating Zhang[1], Wenci Weng[1], Pengxun Han[1], Yuchun Cai[1], Huili Sun[1,2]

[1]Department of Nephrology, Shenzhen Traditional Chinese Medicine Hospital, The Fourth Clinical Medical College of Guangzhou University of Chinese Medicine, Shenzhen 518033, Guangdong, China; [2]Department of Nephrology, Shenzhen Traditional Chinese Medicine Hospital Affiliated to Nanjing University of Chinese Medicine, Shenzhen 518033, Guangdong, China. [*]Equal contributors.

Received March 3, 2025; Accepted July 7, 2025; Epub August 15, 2025; Published August 30, 2025

Abstract: Diabetes is a metabolic disorder involving disruptions in glucose and lipid homeostasis. Skeletal muscle, the primary organ responsible for insulin responsiveness, is crucial for regulating glucose and lipid metabolism. Modulating glucose and lipid metabolism within skeletal muscle to treat diabetes remains an active research area. Artemether, an anti-malarial agent, has significant anti-diabetic and lipid-lowering effects. A type 1 diabetes (T1D) mouse model was induced using streptozotocin. This study comprised three groups: wild-type controls, T1D mice, and T1D mice that received artemether for 8 weeks. Hypoglycemic efficacy was assessed by measuring fasting blood glucose and glycated hemoglobin A1c. Muscle fiber characteristics were analyzed using periodic acid-Schiff staining and immunofluorescence. Alterations in glucose, lipid, pyruvate, and fatty acid metabolism in skeletal muscle were analyzed using immunoblotting, immunofluorescence, and qPCR. In T1D mice, glucose glycolysis and pyruvate metabolism were impaired, whereas fatty acid uptake and use were enhanced. Artemether treatment inhibited pyruvate dehydrogenase kinase 4 activity and activated pyruvate dehydrogenase, promoting aerobic glucose metabolism and suppressing fatty acid metabolism in skeletal muscle. These findings suggest that artemether can alleviate symptoms in T1D mice by modulating glycolipid metabolism in skeletal muscle.

Keywords: Type 1 diabetes mellitus, skeletal muscle, glycolipid metabolism, artemether

Introduction

As modern lifestyles and dietary patterns continue to evolve, the prevalence of diabetes has been on the rise annually. In 2021, approximately 536.6 million (10.5%) of adults aged 20 to 79 years were diagnosed with diabetes. Additionally, there were over 1.2 million cases of type 1 diabetes among children and adolescents. Forecasts indicate that this figure might increase to 12.2% of the adult population by 2045, which is roughly equivalent to 783.2 million individuals [1]. Investigating new diabetes treatments remains crucial.

Skeletal muscle assumes a key role in glucose metabolism by processing 70% to 80% of ingested glucose through storage, oxidation, or glycolysis [2-4]. Skeletal muscle is composed of two primary types of fibers, which are generally classified as oxidative and glycolytic based on their metabolic characteristics [5]. Skeletal muscle's adaptability in using substrates like glucose, fatty acids, and branched-chain amino acids makes it essential for systemic energy homeostasis [6]. However, its role in regulating hyperglycemia and hyperlipemia in diabetes is not fully understood.

Artemisinin derivatives, including artemether, show potential anti-diabetic effects [7-11]. Previous studies indicate that artemether can improve systemic glycolipid metabolism in individuals with diabetes [12-15]. The effect of artemether on glycolipid metabolism in skeletal muscle remains insufficiently understood. We investigated the effects of artemether on glucose and lipid metabolism in a type 1 diabetes mouse model, aiming to explore a novel diabetes treatment approach.

https://doi.org/10.62347/DEHS8462

Materials and methods

Mouse model of T1D

We obtained 8-week-old male C57BL/6J mice (body weight, 22-26 g) from the Guangdong Medical Laboratory Animal Center and maintained them at the Laboratory Animal Research Center, Peking University Shenzhen Graduate School. The environmental conditions were controlled at 20°C to 23°C and 50% to 60% humidity with a 12-hour/12-hour dark/light cycle. The mice had unrestricted access to standard rodent chow and water. Type 1 diabetes was induced in the mice by intraperitoneal injections of streptozotocin (Sigma-Aldrich) at a dosage of 55 mg/kg body weight daily for five days [16]. Mice in the control group received intraperitoneal injections of citrate buffer only. Type 1 diabetic mice were allocated to either the diabetes group (T1D group) or the artemether intervention group (T1D+ artemether group) on the ninth day after the last streptozotocin injection. Regular diet was fed to mice in the control and T1D groups whereas regular diet with 0.8 g/kg artemether was fed to mice in the T1D + artemether group. The intervention period lasted for 8 weeks, after which the mice were euthanized by cervical dislocation under isoflurane anesthesia (3% induction, 1-2% maintenance). The Institutional Animal Care and Use Committee of Guangzhou University of Chinese Medicine approved all procedures, ensuring compliance with relevant guidelines.

Muscle tissue preparation

Muscle tissues were isolated, weighed, and photographed. The quadriceps and gastrocnemius muscles were preserved by snap-freezing in liquid nitrogen. The tibialis anterior muscles used for myofiber cross-sectional area analysis were preserved in 10% formalin. The soleus muscles used for fiber type analysis were preserved by embedding in O.C.T. compound and gradient freezing using liquid nitrogen-cooled isopentane. All muscle types were stored at -80°C.

Periodic acid-Schiff staining and fiber cross-sectional area determination

We evaluated the cross-sectional area of at least 40% of the tibialis anterior fibers using periodic acid-Schiff staining of paraffin-embedded tibialis anterior sections. Briefly, the sections (3 μm in thickness) were baked at 60°C for 2 hours, deparaffinized, stained with periodic acid (15 minutes), rinsed with double-distilled water (10 minutes), incubated in Schiff reagent (15 minutes, in the dark), counterstained with hematoxylin (1 minute), treated with eosin (5 seconds), dehydrated with ethanol/xylene, and sealed with neutral gum. We randomly selected and photographed 8 to 10 fields of view per section under a 40× microscope objective. Fiber cross-sectional area was quantified using ImageJ.

Immunoblotting

The sources of the primary antibodies used to assess changes in protein concentrations related to glycolipid metabolism are as follows. Antibodies for citrate synthase, isocitrate dehydrogenase 3A, oxoglutarate dehydrogenase, hexokinase 2, pyruvate kinase muscle isoform, phosphofructokinase muscle isoform, pyruvate dehydrogenase kinase 4, acyl-coenzyme A (acyl-CoA) dehydrogenases (ACADVL, ACADL, ACADM, ACADS), glyceraldehyde-3-phosphate dehydrogenase, and fatty acid binding protein 3 were sourced from Proteintech. Pyruvate dehydrogenase, phosphorylated pyruvate dehydrogenase (Ser293), and pyruvate dehydrogenase phosphatase 1 antibodies were sourced from Cell Signaling Technology. Experimental methods followed previously published protocols.

Immunofluorescence staining and fiber type determination

For immunofluorescence analysis, paraffin-embedded tibialis anterior muscle sections were dewaxed, rehydrated, and subjected to antigen retrieval using citrate buffer. Then, anti-GLUT4 antibody (IgG2b) was added and incubated overnight at 4°C. O.C.T. compound-embedded soleus muscle sections were fixed with acetone and incubated with a mixture of mouse monoclonal antibodies against myoglobin (MHC-I, BA-F8, IgG2b), MHC-IIa (SC-71, IgG1), and MHC-IIb (BF-F3, IgM) and rabbit-derived laminin (IgG) at room temperature for 3 hours. After the primary antibody incubation, secondary antibodies from Thermo Fisher Scientific were applied for 2 hours at room temperature: Alexa Fluor 488 anti-mouse IgG2b,

Table 1. Primer sequences for real-time quantitative PCR

Gene	Forward primer	Reverse primer
Cs	AAGTTGGCAAAGACGTGTCAG	TACTGCATGACCGTATCCTGG
Idh3a	ACAGGTGACAAGAGGTTTTGC	CTCCCACTGAATAGGTGCTTTG
Ogdh	AGGGCATATCAGATACGAGGG	CTGTGGATGAGATAATGTCAGCG
Tbc1d1	CCTTCGCCAAAAAGTTCGAGG	CGATACACTCGTCAATCAGTGC
Tbc1d4	GCATTCAGGATGAGCCTTTCC	CTCCCACGTACCATAGCCG
Glut4	GTGACTGGAACACTGGTCCTA	CCAGCCACGTTGCATTGTAG
Hk 2	GTGTGCTCCGAGTAAGGGTG	CAGGCATTCGGCAATGTGG
Pfkm	GCCAAAGGTCAGATTGAGGA	CAGGTTCTTCTTGGGGAGAGT
Pkm	GTGGCTCGGCTGAATTTCTCT	CACCGCAACAGGACGGTAG
Pdha1	TCATCACTGCCTATCGAGCAC	GTTGCCTCCATAGAAGTTCTTGG
Pdk4	GCTGGATGTTTGGTGGTTCT	TGCTTTGATTCCTCCCATCC
Pdp1	CGGGCACTGCTACCTATCCTT	ACAATTTGGACGCCTCCTTACT
Mpc1	ACCTCGAAACTGGCTTTTGTT	TCGTAGTTGATAAGTCGTCCTCC
Mpc2	TACCACCGACTCATGGATAAAGT	CACACACCAATCCCCATTTCA
Ldha	ACATTGTCAAGTACAGTCCACAC	TTCCAATTACTCGGTTTTTGGGA
Fabp3	GGAATAGAGTTCGACGAGGTGA	CTCCCTAGTTAGTGTTGTCTCCT
Slc27a1	CGCTTTCTGCGTATCGTCTG	GATGCACGGGATCGTGTCT
Srebp1	CAAGGCCATCGACTACATCCG	CACCACTTCGGGTTTCATGC
Acaca	AATGAACGTGCAATCCGATTTG	ACTCCACATTTGCGTAATTGTTG
Mcd	GCACGTCCGGGAAATGAAC	GCCTCACACTCGCTGATCTT
Gapdh	TGGCCTTCCGTGTTCCTAC	GAGTTGCTGTTGAAGTCGCA

Alexa Fluor 647 anti-mouse IgG1, Alexa Fluor 594 anti-mouse IgM, and Alexa Fluor 405 anti-rabbit IgG. All stained sections were imaged using a confocal microscope, and the composition of fiber types was quantified based on myoglobin subunit expression in accordance with our previously published method [17].

Gene expression analysis

Total RNA from gastrocnemius muscle tissues was purified using a Thermo Fisher Scientific kit. First-strand cDNA synthesis was conducted using deoxynucleoside triphosphates, RNase inhibitor, oligo(dT)12-18 primer, dithiothreitol, and M-MLV reverse transcriptase (Thermo Fisher Scientific), with a reaction at 37°C for 50 minutes followed by termination at 70°C for 15 minutes. qPCR was performed on a QuantStudio 5 PCR system (Thermo Fisher Scientific) using SYBR Green mix with the following steps: an initial denaturation (95°C, 5 minutes), followed by 45 cycles (95°C, 15 seconds; 55°C, 15 seconds; 72°C, 20 seconds). The gene-specific primers (**Table 1**) were provided by Sangon Biotech. mRNA expression levels were normalized to *Gapdh* using the $2^{-\Delta\Delta Ct}$ method.

Triglyceride content determination

The triglyceride content in the quadriceps muscle was assessed using a triglyceride detection kit from Solarbio Science & Technology.

Statistical analysis

Continuous variable data were expressed as mean ± standard deviation. One-way analysis of variance was used for analyzing the differences in data from multiple groups, then Fisher's protected least significant difference test was used for further group comparisons.

Results

Artemether reduces fasting blood glucose and HbA1c concentrations in T1D mice

T1D mice had significantly elevated fasting blood glucose and serum glycated hemoglobin A1c (HbA1c) concentrations compared with controls. Artemether treatment significantly lowered these levels in T1D mice (**Figure 1**).

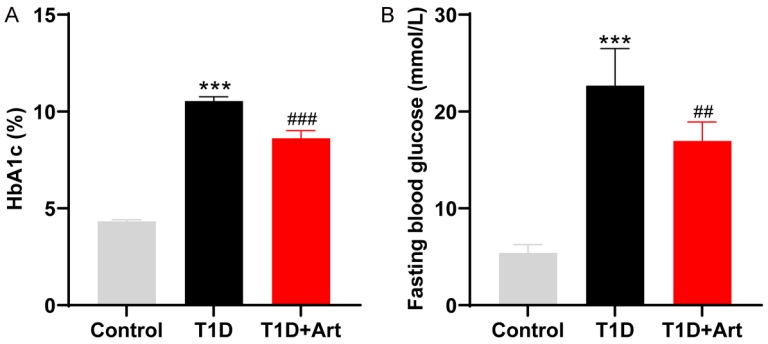

Figure 1. Artemether reduces fasting blood glucose and HbA1c concentrations in T1D mice. A: HbA1c concentration at the experiment's conclusion. B: Fasting blood glucose concentration at 8 weeks after artemether treatment. n=8 per group. ***P<0.001 compared with the control group; ##P<0.01 and ###P<0.001 compared with the T1D group. HbA1c, glycated hemoglobin A1c; T1D, type 1 diabetes.

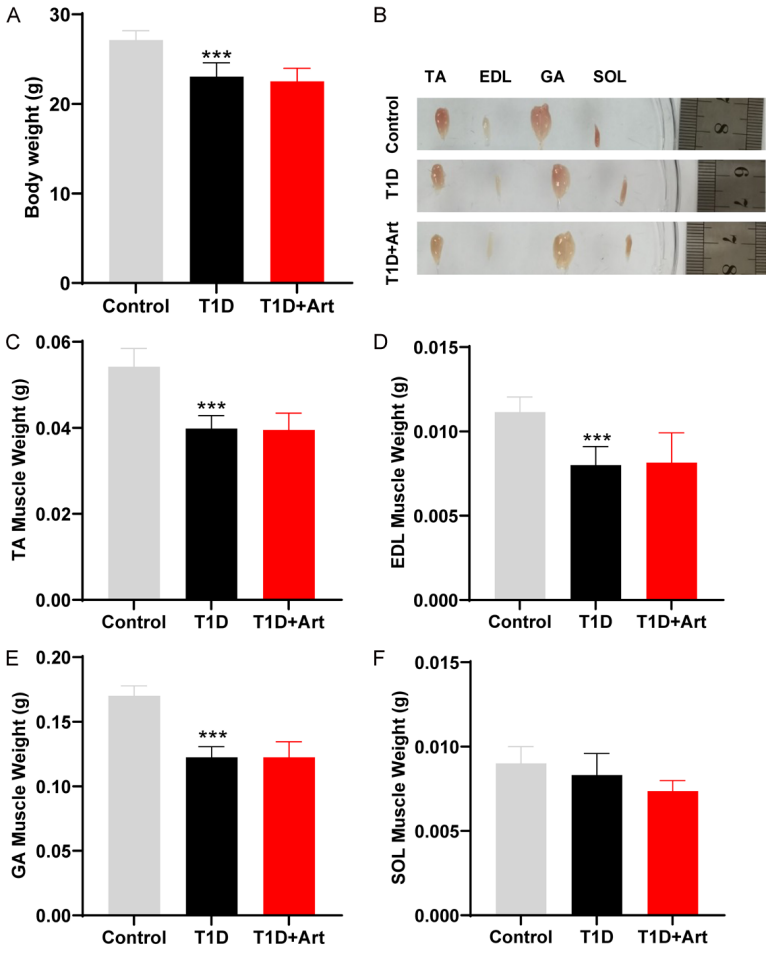

Figure 2. Artemether did not affect body weight and hind limb muscle weight in T1D mice. A: Body weight of mice at 8 weeks after artemether treatment. B: Representative image of lower hind limb muscle. C: Tibialis anterior (TA) muscle weight. D: Extensor digitorum longus (EDL) muscle weight. E: Gastrocnemius (GA) muscle weight. F: Soleus (SOL) muscle weight. n=7-8 per group. ***P<0.001 compared with the control group. T1D, type 1 diabetes.

Artemether did not affect body weight and hind limb muscle weight in T1D mice

The body weight and lower hind limb muscle weight of the T1D mice were significantly lower than the control mice. Notably, artemether intervention did not increase the body weight or muscle weight of T1D mice (**Figure 2**).

Artemether increases the proportion of large oxidative muscle fibers in the skeletal muscle of T1D mice

The cross-sectional area of fibers in the tibialis anterior muscle was lower in T1D mice than in control mice (**Figure 3A**). The number of large muscle fibers (cross-sectional area >1250 μm^2) was also significantly lower in T1D mice than in control mice (**Figure 3B**, **3C**, **3F**). Interestingly, the composition of the muscle fiber type changed, which manifested as an increase in oxidative fibers and a decrease in glycolytic type II fibers in T1D mice compared with control mice (**Figure 3D**, **3E**, **3G**). Artemether treatment further increased the aforementioned changes in T1D mice.

Key enzymes of the tricarboxylic acid cycle are unchanged in the skeletal muscle of T1D mice

Citrate synthase, isocitrate dehydrogenase 3A, and oxoglutarate dehydrogenase are enzymes that regulate the tricarboxylic acid (TCA) cycle within cells. Citrate synthase initiates the TCA cycle in a rate-limiting manner, synthesizing citrate from acetyl-CoA and oxaloacetic acid within mitochondrial membranes.

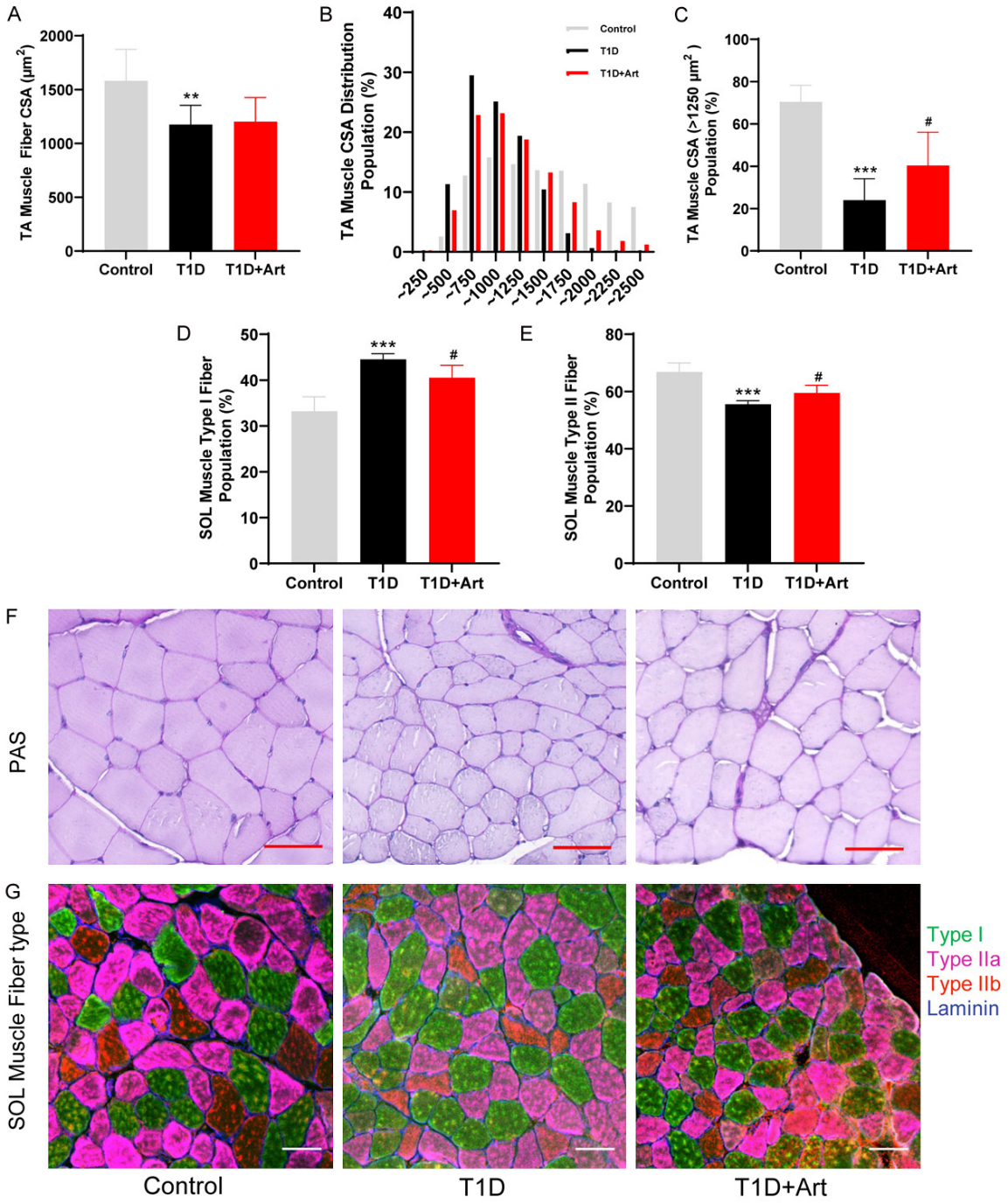

Figure 3. Artemether increases the proportion of large oxidative muscle fibers in the skeletal muscle of T1D mice. A: Cross-sectional area (CSA) of tibialis anterior (TA) muscle fiber. B: TA muscle fiber CSA distribution population. C: TA muscle fiber CSA >1250 μm^2 distribution population. D: Soleus (SOL) muscle type I fiber population. E: SOL muscle type II (IIa + IIb) fiber population. F: Representative images illustrating changes in fiber size (periodic acid-Schiff stained; scale bar, 50 μm). G: Representative images of muscle fiber type composition (Scale bar, 50 um). n=4-8 per group. $^{**}P$<0.01 and $^{***}P$<0.001 compared with the control group; $^{\#}P$<0.05 compared with the T1D group. T1D, type 1 diabetes.

Isocitrate dehydrogenase 3A limits the decarboxylation rate of isocitrate into α-ketoglutarate. Oxoglutarate dehydrogenase converts α-ketoglutarate to succinyl-CoA while generating NADH, which is then used for ATP production through oxidative phosphorylation. In our

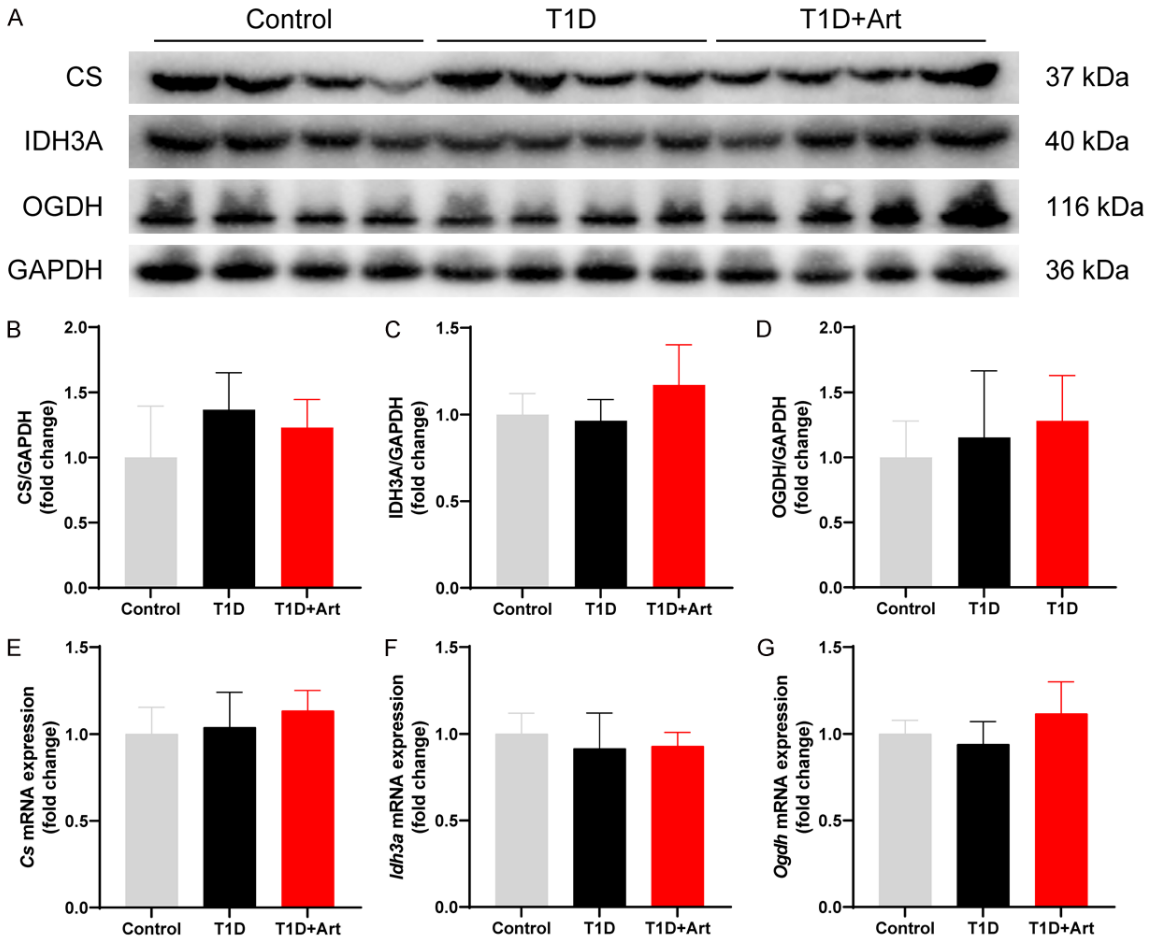

Figure 4. Key enzymes of the tricarboxylic acid cycle are unchanged in the skeletal muscle of T1D mice. A: Western blot images of citrate synthase (CS), isocitrate dehydrogenase 3A (IDH3A), and oxoglutarate dehydrogenase (OGDH) in gastrocnemius (GA) muscle for each group. B-D: Normalized fold change in CS, IDH3A, and OGDH protein expression after normalization to glyceraldehyde-3-phosphate dehydrogenase (GAPDH) expression. E-G: Relative mRNA expression of *Cs, Idh3a and Ogdh* in the GA muscle for each group. n=6-8 per group. T1D, type 1 diabetes.

study, changes in expression of citrate synthase, isocitrate dehydrogenase 3A, and oxoglutarate dehydrogenase in skeletal muscle of T1D mice were insignificant compared with the control group, as measured by immunoblot and relative mRNA expression (**Figure 4**).

Artemether ameliorates impaired glucose transport in the skeletal muscle of T1D mice

GLUT4 is the primary glucose transporter in skeletal muscles, enabling glucose uptake by translocating it from intracellular compartments to the plasma membrane. This process can be aided by TBC1D1 and TBC1D4. Although *Tbc1d1* and *Tbc1d4* mRNA expression did not differ significantly between groups, *Glut4* mRNA levels were notably reduced in T1D mice compared with controls (**Figure 5A-C**). Immunofluorescence (**Figure 5D**) showed reduced GLUT4 translocation to the muscle cell membrane in T1D mice compared with control mice. In contrast, artemether treatment increased *Glut4* mRNA expression (**Figure 5C**) and enhanced translocation of GLUT4 to the muscle cell membrane (**Figure 5D**).

Artemether enhances glucose glycolysis in the skeletal muscle of T1D mice

T1D mice and control mice had similar protein expression of hexokinase 2 and phosphofructokinase muscle isoform in skeletal muscle, as measured by immunoblot assay. However, pyruvate kinase muscle isoform protein expression was significantly reduced in T1D mice com-

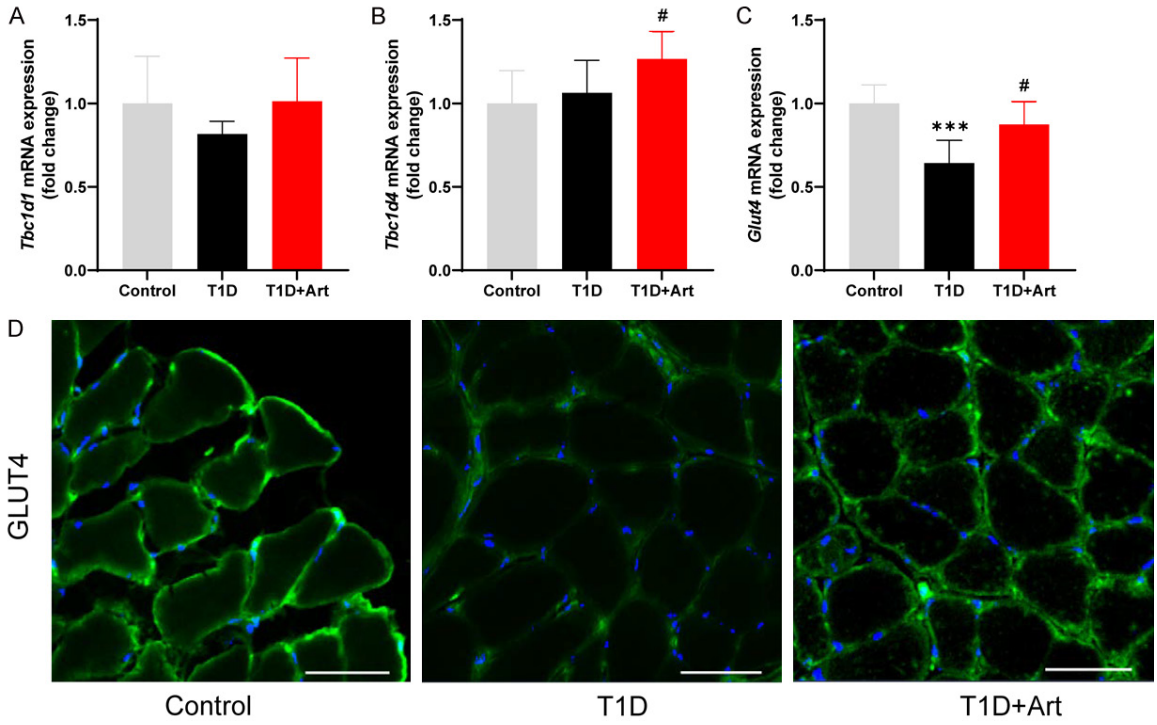

Figure 5. Artemether ameliorates impaired glucose transport in the skeletal muscle of T1D mice. A-C: Relative mRNA expression of *Tbc1d1, Tbc1d4,* and *Glut4* in the gastrocnemius (GA) muscle for each group. D: Representative images of GLUT4 in the skeletal muscle of each group (Scale bar, 50 um). n=6 per group. ***P<0.001 compared to the control group; #P<0.05 compared with the T1D group. T1D, type 1 diabetes.

pared with control mice. Following artemether administration, the protein expression of hexokinase 2, phosphofructokinase muscle isoform, and pyruvate kinase muscle isoform trended upward but did not reach statistical significance (**Figure 6A-D**). At the mRNA level, the expression of *Hk2* and *Pfkm* in the skeletal muscle of T1D mice was markedly decreased compared with the control group. In contrast, artemether treatment increased mRNA expression of *Hk2* and *Pfkm*, whereas the mRNA expression of *Pkm* remained stable (**Figure 6E-G**).

Artemether enhances aerobic pyruvate metabolism in the skeletal muscle of T1D mice

Immunoblot assays revealed that T1D mice had significantly elevated ratios of phosphorylated pyruvate dehydrogenase (Ser293) to pyruvate dehydrogenase and pyruvate dehydrogenase kinase 4 in skeletal muscle, which were mitigated by artemether treatment (**Figure 7A-C**). Artemether also reversed the changes in mRNA levels of *Pdh* and *Pdk4* in T1D mice (**Figure 7E**, **7F**). No remarkable difference was noted in either pyruvate dehydrogenase phosphatase 1 protein or mRNA expression across the three groups (**Figure 7D**, **7G**). Compared with controls, mRNA expression of mitochondrial pyruvate carriers *Mpc1* and *Mpc2* decreased in T1D mice; artemether treatment increased their mRNA expression (**Figure 7H**, **7I**). Additionally, *Ldha* mRNA levels were higher in T1D mouse skeletal muscle but normalized after artemether treatment (**Figure 7J**).

Artemether decreases fatty acid transport and restores fatty acid synthesis in the skeletal muscle of T1D mice

Fatty acid binding protein 3 [18] and SLC27A1 [19] play crucial roles in the transmembrane transport of fatty acids into muscle cells. **Figure 8A-D** illustrates that the protein and mRNA expression of fatty acid binding protein 3 and mRNA expression of *Slc27a1* was elevated in T1D group compared with control mice, and artemether treatment reduced fatty acid binding protein 3 protein expression. The expression of the sterol regulatory element binding protein 1, which mediates de novo fatty acid

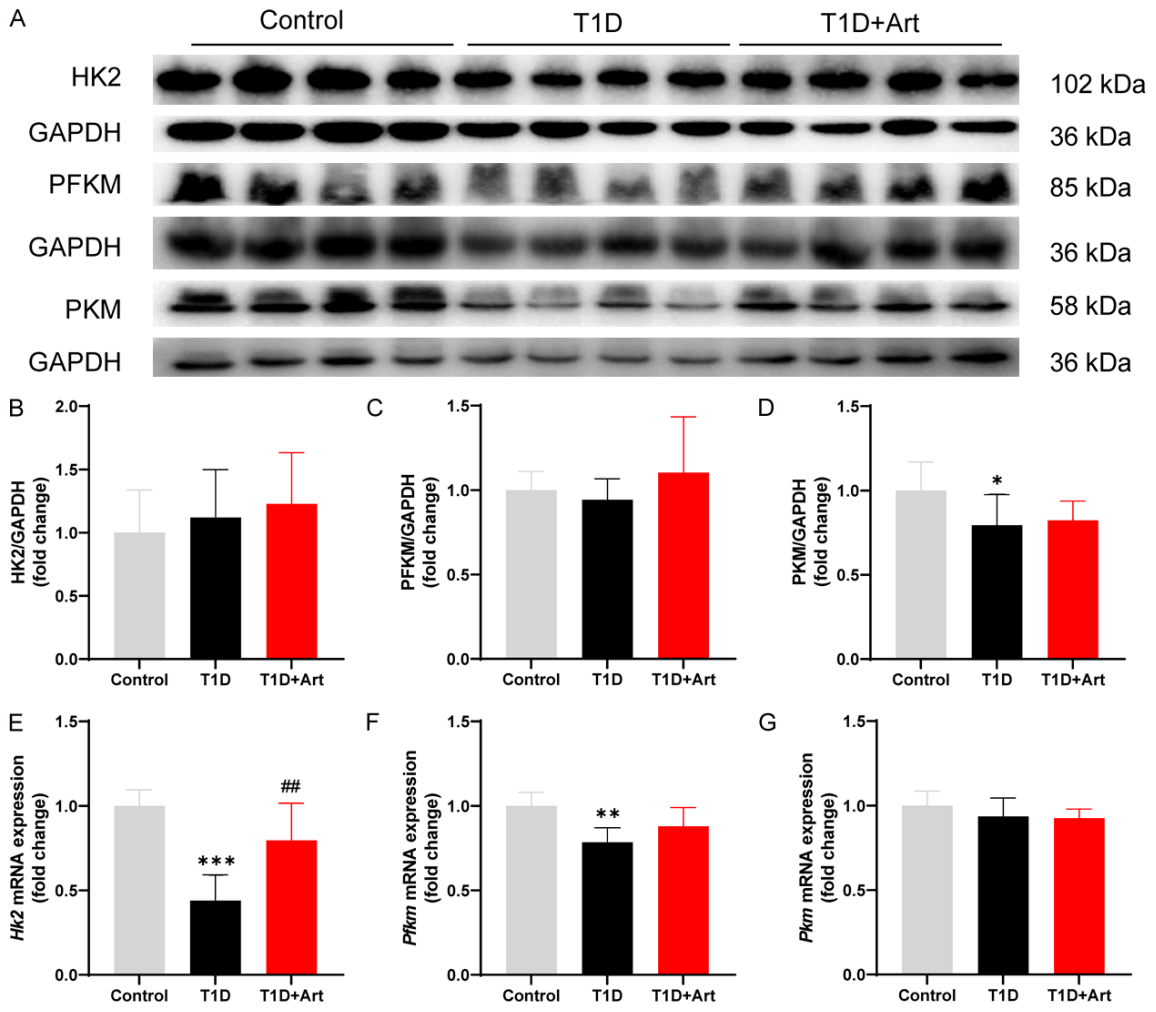

Figure 6. Artemether enhances glucose glycolysis in the skeletal muscle of T1D mice. A: Western blot images of hexokinase 2 (HK2), phosphofructokinase muscle isoform (PFKM), and pyruvate kinase muscle isoform (PKM) expression in gastrocnemius (GA) muscle for each group. B-D: Fold change in HK2, PFKM, and PKM protein expression after normalization toglyceraldehyde-3-phosphate dehydrogenase (GAPDH) expression. E-G: Relative mRNA expression of *Hk2*, *Pfkm*, and *Pkm* in the GA muscle for each group. n=6-8 per group. $^{*}P<0.05$, $^{**}P<0.01$ and $^{***}P<0.001$ compared with the control group; $^{\#}P<0.05$ and $^{\#\#}P<0.01$ compared with the T1D group. T1D, type 1 diabetes.

synthesis, is sensitive to insulin [20]. As shown in **Figure 8E**, expression of *Srebp1* mRNA dramatically decreased in T1D mice and was upregulated by artemether treatment.

Artemether suppresses active fatty acid metabolism in the skeletal muscle of T1D mice

Acyl-CoA dehydrogenases (ACADVL, ACADL, ACADM, and ACADS) initiate the beta-oxidation of fatty acids. The protein expression of these enzymes was elevated in the skeletal muscle of T1D mice, as determined by immunoblot (**Figure 9A-E**). Malonyl-CoA, which is involved in inhibiting fatty acid beta-oxidation, is regulated by two important enzymes, acetyl-CoA carboxylase [21] and malonyl-CoA decarboxylase [22]. **Figure 9F** and **9G** illustrates decreased *Acaca* and increased *Mcd* mRNA expression in T1D mice. The triglyceride content in muscle tissue and respiratory exchange ratio also decreased in T1D mice (**Figure 9H**, **9I**). Artemether treatment partially reversed these changes (**Figure 9**).

Discussion

This study demonstrated that the fuel substrate of skeletal muscle in individuals with T1D shifts from glucose to fatty acids. Artemether may

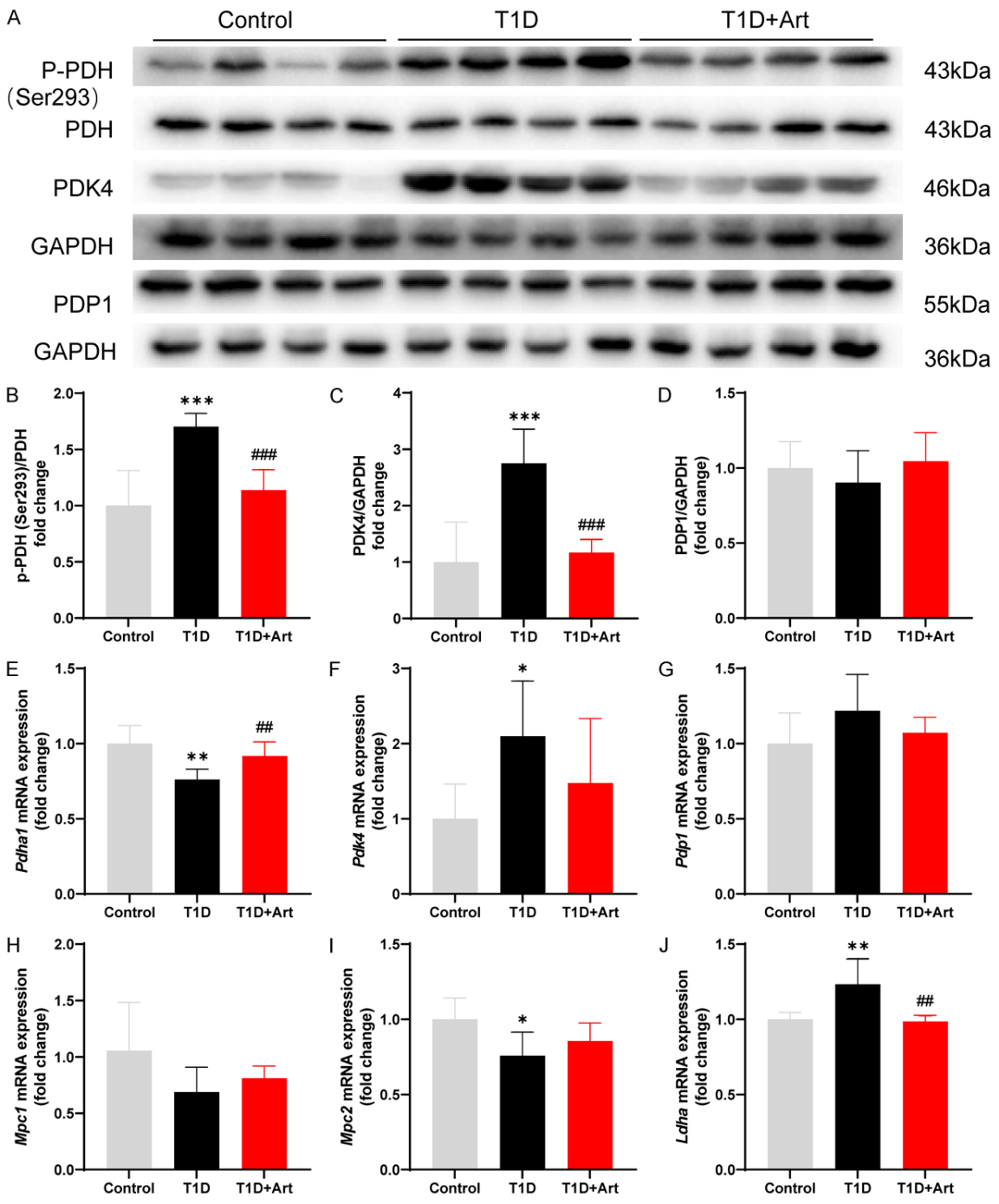

Figure 7. Artemether enhances aerobic pyruvate metabolism in the skeletal muscle of T1D mice. A: Western blot images of phosphorylated pyruvate dehydrogenase (p-PDH; Ser293), pyruvate dehydrogenase (PDH), pyruvate dehydrogenase kinase 4 (PDK4), and pyruvate dehydrogenase phosphatase 1 (PDP1) expression in gastrocnemius (GA) for each group. B: Expression ratio of p-PDH (Ser293) to PDH. C, D: Western blot quantification analysis of PDK4 and PDP1 expression. E-J: Relative mRNA expression of *Pdh*, *Pdk4*, *Pdp1*, *Mpc1*, *Mpc2*, and *Ldha* in the GA muscle for each group. n=6-8 per group. $^{*}P<0.05$, $^{**}P<0.01$, and $^{***}P<0.001$ compared with the control group; $^{\#\#}P<0.01$ and $^{\#\#\#}P<0.001$ compared with the T1D group. T1D, type 1 diabetes.

exert its hypoglycemic effect in T1D mice by modulating glucose and fatty acid metabolism in the skeletal muscle.

Skeletal muscle has a high energy demand due to physiological activities and is sensitive to insulin, allowing it to metabolize both glucose

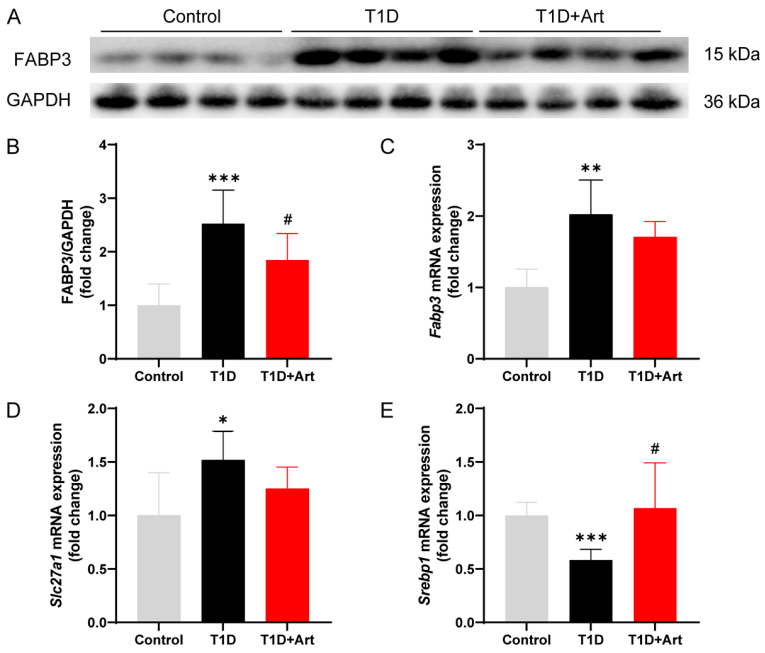

Figure 8. Artemether decreases fatty acid transport and restores fatty acid synthesis in the skeletal muscle of T1D mice. A, B: Representative western blot images and quantification analysis of fatty acid binding protein 3 (FABP3) expression. C, D: Relative mRNA levels of *Fabp3* and *Slc27a1* in the gastrocnemius (GA) muscle for each group. E: Relative mRNA expression of *Srebp1* in the GA muscle for each group. n=6-8 per group. **P*<0.05, ***P*<0.01, and ****P*<0.001 compared with the control group; #*P*<0.05 compared with the T1D group. T1D, type 1 diabetes.

and lipids. This metabolic flexibility is crucial for maintaining energy homeostasis within the body, particularly glucose homeostasis. Skeletal muscle fibers can be divided into four types, based on contraction speed, metabolic capacity, and myosin heavy chain expression: slow oxidative (type I), fast oxidative (type IIa), fast oxidative and glycolytic (type IIx), and fast glycolytic (type IIb) [23]. The distinct metabolic properties of these fiber types influence their substrate selection [24]. Red slow-twitch type I fibers are abundant in myoglobin as well as mitochondrial and oxidative enzymes, enabling these fibers to oxidize fatty acids more efficiently than their fast-twitch counterparts [25, 26]. Both endurance training [27] and fasting [28] increase the quantity of type I fibers in muscle and induce a shift in fuel use from glucose to fatty acids. Similarly, we found the proportion of type I muscle fibers in T1D mice was notably increased compared with control mice. In contrast, the proportion of type II muscle fibers was decreased in T1D mice, which was primarily limited by glucose delivery and transport [29]. We propose that there may be a dynamic interchange between glucose and fatty acids as energy substrates within the skeletal muscle of T1D mice that can potentially be regulated by artemether. The primary sources of energy supply in skeletal muscle derive from both glucose and fatty acids through the generation of acetyl-CoA [30], which enters the TCA cycle to provide energy via oxidative phosphorylation. Our analysis of the key enzymes in the TCA cycle revealed no significant differences across the three groups.

GLUT4 is the predominant isoform found in skeletal muscles [31]; *Glut4* mRNA expression was decreased in T1D mice compared with control mice. Immunofluorescence analysis revealed that the translocation of GLUT4 to the cell membrane was reduced in T1D mice, suggesting that glucose uptake was impaired in these mice. The use of glucose by skeletal muscle encompasses aerobic oxidative phosphorylation and anaerobic oxidation, as well as glycogen synthesis. Among them, aerobic oxidative phosphorylation serves as the primary mechanism for skeletal muscle to use glucose [3]. The pyruvate dehydrogenase complex controls glucose oxidation by irreversibly converting pyruvate to acetyl-CoA [32]; this conversion is negatively regulated by phosphorylation of pyruvate dehydrogenase kinases 1-4. Our study identified a notable rise in pyruvate dehydrogenase kinase 4, the main isoform in skeletal muscle, and phosphorylated pyruvate dehydrogenase in the skeletal muscle of T1D mice, suggesting decreased conversion of pyruvate to acetyl-CoA. Pyruvate dehydrogenase kinase inhibitors are capable of reducing fasting blood glucose concentration in rodent models and humans [33], independent of insulin action [34]. In our study, consistent with our previous research [16], artemether strongly inhibited pyruvate dehydrogenase kinase 4, enhanced the activity of pyruvate dehydrogenase, and converted pyruvate into acetyl-CoA, thereby

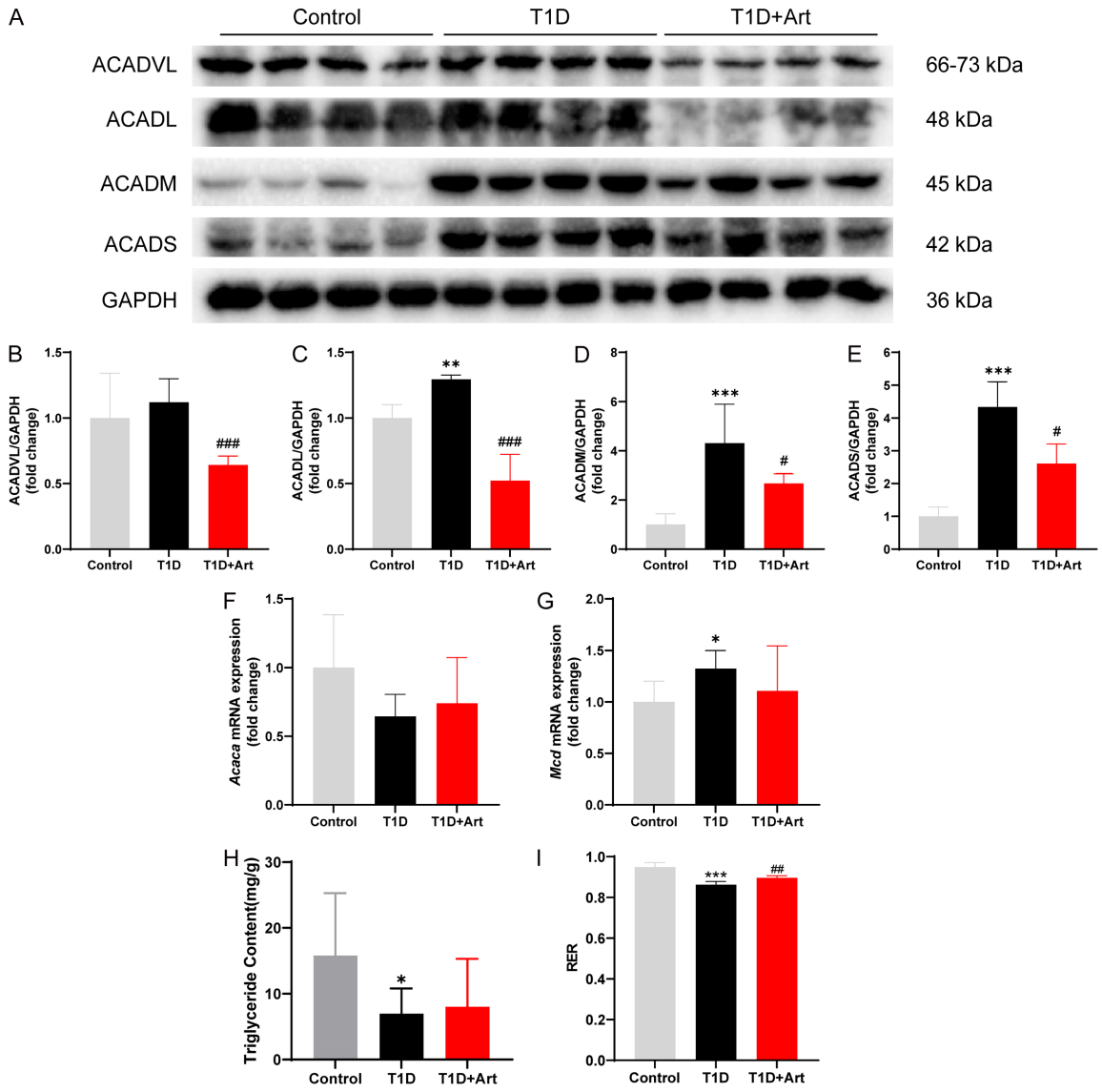

Figure 9. Artemether suppresses active fatty acid metabolism in the skeletal muscle of T1D mice. A: Western blot images of acyl-coenzyme A dehydrogenases (ACADVL, ACADL, ACADM, ACADS) expression in gastrocnemius (GA) muscle for each group. B-E: Western blot quantification analysis of ACADVL, ACADL, ACADM, ACADS proteins expression. F, G: Relative mRNA expression of *Acaca* and *Mcd*. H: Quadriceps (QF) muscle triglyceride content for each group. I: Respiratory exchange ratio (RER) for each group. n=4-8 per group. **P*<0.05, ***P*<0.01, and ****P*<0.001 compared with the control group; $^{\#}$*P*<0.05 and $^{\#\#\#}$*P*<0.001 compared with the T1D group. T1D, type 1 diabetes.

enhancing the use of glucose in skeletal muscle of T1D mice.

Pyruvate dehydrogenase kinase shifts fuel oxidation from carbohydrates to fatty acids and is more active in oxidative muscles compared with glycolytic muscles [5, 35]. When glucose availability is limited, fatty acids serve as a crucial source of acetyl-CoA. Despite sufficient glucose levels, fatty acid beta-oxidation continues to supply the energy fuel for the heart, skeletal muscles, and kidneys [36]. In our study, we discovered that the protein and mRNA expression levels of fatty acid binding protein 3 and SLC27A1 were elevated in skeletal muscle. This result implies that muscle cells have an increased capacity for fatty acid uptake. In skeletal muscle, insulin and glucose activate de novo fatty acid synthesis through sterol regulatory element binding protein 1 [37, 38]. The

mRNA expression of *Srebp*1 was decreased in the skeletal muscle of T1D mice in this study, which suggests that fatty acid synthesis is diminished in these mice.

An increase in fatty acyl-CoA dehydrogenase levels in the skeletal muscle of T1D mice suggests elevated beta-oxidation of fatty acids [39]. As a crucial regulator of cellular lipid metabolism, acetyl-CoA carboxylase catalyzes the transformation of acetyl-CoA into malonyl-CoA. Malonyl-CoA decarboxylase modulates malonyl-CoA levels by facilitating its breakdown into acetyl-CoA and carbon dioxide while inhibiting acetyl-CoA carboxylase activity [40]. Our findings demonstrate a downregulation of acetyl-CoA carboxylase, which may decrease production of malonyl-CoA. A decreased production of malonyl-CoA, combined with the upregulation of malonyl-CoA decarboxylase, further inhibits malonyl-CoA generation. As a result, the decreased inhibition of carnitine palmitoyltransferase I by malonyl-CoA enhances fatty acid oxidation [41]. Our observed decreases in respiratory exchange ratio and triglyceride content within skeletal muscle in T1D mice provide additional evidence that muscle tissue relies on fatty acid metabolism to compensate for inadequate glucose metabolism in T1D mice. Furthermore, our results indicate that artemether intervention suppresses fatty acid metabolism by downregulating both uptake and use of fatty acids.

In summary, skeletal muscle has metabolic flexibility, transitioning its fuel substrates from glucose to fatty acids in the context of a T1D mouse model. Artemether induces hypoglycemia by inhibiting the activity of pyruvate dehydrogenase kinase 4, thereby activating pyruvate dehydrogenase. This process enhances the aerobic oxidation of glucose within skeletal muscle while simultaneously inhibiting fatty acid metabolism.

Acknowledgements

The present study was supported by the Shenzhen Science and Technology Project (grant no. JCYJ20220531092405011; JCYJ201908121-83603627), the Shenzhen Fund for Guangdong Provincial High-level Clinical Key Specialties, Shenzhen High-level Hospital Construction Fund and Sanming Project of Medicine in Shenzhen (No. SZZYSM202311004).

Disclosure of conflict of interest

None.

Address correspondence to: Huili Sun, Department of Nephrology, Shenzhen Traditional Chinese Medicine Hospital Affiliated to Nanjing University of Chinese Medicine, No. 1 Fuhua Road, Futian District, Shenzhen 518033, Guangdong, China. E-mail: sunhuili2011@126.com; shl1412@gzucm.edu.cn; Yuchun Cai, Department of Nephrology, Shenzhen Traditional Chinese Medicine Hospital, The Fourth Clinical Medical College of Guangzhou University of Chinese Medicine, No. 1 Fuhua Road, Futian District, Shenzhen 518033, Guangdong, China. E-mail: caiyuchun2021@163.com

References

[1] Gregory GA, Robinson TIG, Linklater SE, Wang F, Colagiuri S, de Beaufort C, Donaghue KC; International Diabetes Federation Diabetes Atlas Type 1 Diabetes in Adults Special Interest Group, Magliano DJ, Maniam J, Orchard TJ, Rai P and Ogle GD. Global incidence, prevalence, and mortality of type 1 diabetes in 2021 with projection to 2040: a modelling study. Lancet Diabetes Endocrinol 2022; 10: 741-760.

[2] Sun Z, Liu L, Liu N and Liu Y. Muscular response and adaptation to diabetes mellitus. Front Biosci 2008; 13: 4765-4794.

[3] Egan B and Zierath JR. Exercise metabolism and the molecular regulation of skeletal muscle adaptation. Cell Metab 2013; 17: 162-184.

[4] DeFronzo RA, Jacot E, Jequier E, Maeder E, Wahren J and Felber JP. The effect of insulin on the disposal of intravenous glucose. Results from indirect calorimetry and hepatic and femoral venous catheterization. Diabetes 1981; 30: 1000-1007.

[5] Zumbaugh MD, Johnson SE, Shi TH and Gerrard DE. Molecular and biochemical regulation of skeletal muscle metabolism. J Anim Sci 2022; 100: skac035.

[6] Shoemaker ME, Pereira SL, Mustad VA, Gillen ZM, McKay BD, Lopez-Pedrosa JM, Rueda R and Cramer JT. Differences in muscle energy metabolism and metabolic flexibility between sarcopenic and nonsarcopenic older adults. J Cachexia Sarcopenia Muscle 2022; 13: 1224-1237.

[7] Wu T, Feng H, He M, Yue R and Wu S. Efficacy of artemisinin and its derivatives in animal models of type 2 diabetes mellitus: a systematic review and meta-analysis. Pharmacol Res 2022; 175: 105994.

[8] Chen Y, Weng W, Zhang H, Rong G, Yu X, Wei Q, Shao M, Cai Y, Han P and Sun H. Combination

therapy with artemether and enalapril improves type 1 diabetic nephropathy through enhancing antioxidant defense. Am J Transl Res 2022; 14: 211-222.
[9] Rong G, Weng W, Huang J, Chen Y, Yu X, Yuan R, Gu X, Wu X, Cai Y, Han P, Shao M, Sun H and Ge N. Artemether alleviates diabetic kidney disease by modulating amino acid metabolism. Biomed Res Int 2022; 2022: 7339611.
[10] Han P, Wang Y, Zhan H, Weng W, Yu X, Ge N, Wang W, Song G, Yi T, Li S, Shao M and Sun H. Artemether ameliorates type 2 diabetic kidney disease by increasing mitochondrial pyruvate carrier content in db/db mice. Am J Transl Res 2019; 11: 1389-1402.
[11] Ma N, Zhang Z, Liao F, Jiang T and Tu Y. The birth of artemisinin. Pharmacol Ther 2020; 216: 107658.
[12] Bai X, Pei R, Lei W, Zhao M, Zhang J, Tian L and Shang J. Antidiabetic effect of artemether in Db/Db mice involves regulation of AMPK and PI3K/Akt pathways. Front Endocrinol (Lausanne) 2020; 11: 568864.
[13] Fu W, Ma Y, Li L, Liu J, Fu L, Guo Y, Zhang Z, Li J and Jiang H. Artemether regulates metaflammation to improve glycolipid metabolism in db/db mice. Diabetes Metab Syndr Obes 2020; 13: 1703-1713.
[14] Guo Y, Fu W, Xin Y, Bai J, Peng H, Fu L, Liu J, Li L, Ma Y and Jiang H. Antidiabetic and antiobesity effects of artemether in db/db mice. Biomed Res Int 2018; 2018: 8639523.
[15] Weng W, Shen L, Yu X, Yuan R, Shao M, Han P and Sun H. Artemether regulates liver glycogen and lipid utilization through mitochondrial pyruvate oxidation in db/db mice. Am J Transl Res 2024; 16: 27-38.
[16] Wang Y, Han P, Wang M, Weng W, Zhan H, Yu X, Yuan C, Shao M and Sun H. Artemether improves type 1 diabetic kidney disease by regulating mitochondrial function. Am J Transl Res 2019; 11: 3879-3889.
[17] Cai Y, Zhan H, Weng W, Wang Y, Han P, Yu X, Shao M and Sun H. Niclosamide ethanolamine ameliorates diabetes-related muscle wasting by inhibiting autophagy. Skelet Muscle 2021; 11: 15.
[18] Lee SM, Lee SH, Jung Y, Lee Y, Yoon JH, Choi JY, Hwang CY, Son YH, Park SS, Hwang GS, Lee KP and Kwon KS. FABP3-mediated membrane lipid saturation alters fluidity and induces ER stress in skeletal muscle with aging. Nat Commun 2020; 11: 5661.
[19] Glatz JF, Luiken JJ and Bonen A. Membrane fatty acid transporters as regulators of lipid metabolism: implications for metabolic disease. Physiol Rev 2010; 90: 367-417.
[20] Eberlé D, Hegarty B, Bossard P, Ferré P and Foufelle F. SREBP transcription factors: master regulators of lipid homeostasis. Biochimie 2004; 86: 839-848.
[21] Yeudall S, Upchurch CM, Seegren PV, Pavelec CM, Greulich J, Lemke MC, Harris TE, Desai BN, Hoehn KL and Leitinger N. Macrophage acetyl-CoA carboxylase regulates acute inflammation through control of glucose and lipid metabolism. Sci Adv 2022; 8: eabq1984.
[22] Guilherme A, Rowland LA, Wetoska N, Tsagkaraki E, Santos KB, Bedard AH, Henriques F, Kelly M, Munroe S, Pedersen DJ, Ilkayeva OR, Koves TR, Tauer L, Pan M, Han X, Kim JK, Newgard CB, Muoio DM and Czech MP. Acetyl-CoA carboxylase 1 is a suppressor of the adipocyte thermogenic program. Cell Rep 2023; 42: 112488.
[23] Schiaffino S and Reggiani C. Fiber types in mammalian skeletal muscles. Physiol Rev 2011; 91: 1447-1531.
[24] Actis Dato V, Lange S and Cho Y. Metabolic flexibility of the heart: the role of fatty acid metabolism in health, heart failure, and cardiometabolic diseases. Int J Mol Sci 2024; 25: 1211.
[25] Komiya Y, Sawano S, Mashima D, Ichitsubo R, Nakamura M, Tatsumi R, Ikeuchi Y and Mizunoya W. Mouse soleus (slow) muscle shows greater intramyocellular lipid droplet accumulation than EDL (fast) muscle: fiber type-specific analysis. J Muscle Res Cell Motil 2017; 38: 163-173.
[26] Rakus D, Gizak A, Deshmukh A and Wiśniewski JR. Absolute quantitative profiling of the key metabolic pathways in slow and fast skeletal muscle. J Proteome Res 2015; 14: 1400-1411.
[27] Abernethy PJ, Thayer R and Taylor AW. Acute and chronic responses of skeletal muscle to endurance and sprint exercise. A review. Sports Med 1990; 10: 365-389.
[28] de Lange P, Ragni M, Silvestri E, Moreno M, Schiavo L, Lombardi A, Farina P, Feola A, Goglia F and Lanni A. Combined cDNA array/RT-PCR analysis of gene expression profile in rat gastrocnemius muscle: relation to its adaptive function in energy metabolism during fasting. Faseb J 2004; 18: 350-352.
[29] Halseth AE, Bracy DP and Wasserman DH. Functional limitations to glucose uptake in muscles comprised of different fiber types. Am J Physiol Endocrinol Metab 2001; 280: E994-999.
[30] Alghannam AF, Ghaith MM and Alhussain MH. Regulation of energy substrate metabolism in endurance exercise. Int J Environ Res Public Health 2021; 18: 4963.
[31] Hulett NA, Scalzo RL and Reusch JEB. Glucose uptake by skeletal muscle within the contexts of type 2 diabetes and exercise: an integrated approach. Nutrients 2022; 14: 647.

[32] Gopal K, Abdualkader AM, Li X, Greenwell AA, Karwi QG, Altamimi TR, Saed C, Uddin GM, Darwesh AM, Jamieson KL, Kim R, Eaton F, Seubert JM, Lopaschuk GD, Ussher JR and Al Batran R. Loss of muscle PDH induces lactic acidosis and adaptive anaplerotic compensation via pyruvate-alanine cycling and glutaminolysis. J Biol Chem 2023; 299: 105375.

[33] Wang X, Shen X, Yan Y and Li H. Pyruvate dehydrogenase kinases (PDKs): an overview toward clinical applications. Biosci Rep 2021; 41: BSR20204402.

[34] Small L, Brandon AE, Quek LE, Krycer JR, James DE, Turner N and Cooney GJ. Acute activation of pyruvate dehydrogenase increases glucose oxidation in muscle without changing glucose uptake. Am J Physiol Endocrinol Metab 2018; 315: E258-e266.

[35] Holness MJ, Kraus A, Harris RA and Sugden MC. Targeted upregulation of pyruvate dehydrogenase kinase (PDK)-4 in slow-twitch skeletal muscle underlies the stable modification of the regulatory characteristics of PDK induced by high-fat feeding. Diabetes 2000; 49: 775-781.

[36] Houten SM, Violante S, Ventura FV and Wanders RJ. The biochemistry and physiology of mitochondrial fatty acid β-oxidation and its genetic disorders. Annu Rev Physiol 2016; 78: 23-44.

[37] Takagi H, Ikehara T, Hashimoto K, Tanimoto K, Shimazaki A, Kashiwagi Y, Sakamoto S and Yukioka H. Acetyl-CoA carboxylase 2 inhibition reduces skeletal muscle bioactive lipid content and attenuates progression of type 2 diabetes in Zucker diabetic fatty rats. Eur J Pharmacol 2021; 910: 174451.

[38] Guillet-Deniau I, Pichard AL, Koné A, Esnous C, Nieruchalski M, Girard J and Prip-Buus C. Glucose induces de novo lipogenesis in rat muscle satellite cells through a sterol-regulatory-element-binding-protein-1c-dependent pathway. J Cell Sci 2004; 117: 1937-1944.

[39] Eaton S, Bartlett K and Pourfarzam M. Mammalian mitochondrial beta-oxidation. Biochem J 1996; 320: 345-357.

[40] Bouzakri K, Austin R, Rune A, Lassman ME, Garcia-Roves PM, Berger JP, Krook A, Chibalin AV, Zhang BB and Zierath JR. Malonyl CoenzymeA decarboxylase regulates lipid and glucose metabolism in human skeletal muscle. Diabetes 2008; 57: 1508-1516.

[41] Vavrova E, Lenoir V, Alves-Guerra MC, Denis RG, Castel J, Esnous C, Dyck JR, Luquet S, Metzger D, Bouillaud F and Prip-Buus C. Muscle expression of a malonyl-CoA-insensitive carnitine palmitoyltransferase-1 protects mice against high-fat/high-sucrose diet-induced insulin resistance. Am J Physiol Endocrinol Metab 2016; 311: E649-660.